Optics & Laser Technology 156 (2022) 108567

Contents lists available at ScienceDirect

Optics and Laser Technology

journal homepage: www.elsevier.com/locate/optlastec

Mueller matrix polarimetric analysis applied to characterize the physical parameters of a twisted-nematic liquid–crystal modulator

Esther Nabadda [a], Guadalupe López-Morales [a,b], David Marco [a], María del Mar Sánchez-López [a,c], Ignacio Moreno [a,d,*]

[a] Instituto de Bioingeniería, Universidad Miguel Hernández de Elche, 03202 Elche, Spain
[b] Instituto de Investigación e Innovación en Energías Renovables, Universidad de las Ciencias y las Artes de Chiapas, Mexico
[c] Departamento de Física Aplicada, Universidad Miguel Hernández de Elche, 03202 Elche, Spain
[d] Departamento de Ciencia de Materiales, Óptica y Tecnología Electrónica, Universidad Miguel Hernández de Elche, 03202 Elche, Spain

ARTICLE INFO

Keywords:
Twisted Nematic Liquid-Crystal Modulators
Polarimetry
Mueller Matrix
Linear and Circular Retardance

ABSTRACT

This work presents a complete polarimetric study of a twisted-nematic (TN) liquid–crystal (LC) cell. We review the physical models that describe the cell and analyze the different modulation regimes. We extend the usual Jones matrix approach, where these microscopic physical models were developed, to the corresponding Mueller matrix approach. This polarimetric analysis is then used to obtain the effective linear and circular retardance components of the cell and to characterize its physical parameters like the twist angle, the orientation of the LC director axis and the maximum retardance. The technique simplifies previous approaches with the advantage of employing a single wavelength. Noteworthy, it also resolves the ambiguities in the determination of the physical parameters. Experimental evidence of the effectiveness in predicting the optical modulation is shown for a single-pixel TN-LC cell. Finally, a simplified procedure is presented under the assumption that the TN-LC cell is a pure retarder component, which is useful to perform a rapid calibration of the device.

1. Introduction

Twisted-nematic liquid crystals (TN-LC) constitute a well-established and widely employed display technology. They are also useful to build optical phase modulators, either as single cell devices or in the form of pixelated spatial light modulators (SLMs) [1]. They are linear retarders with special structures where the LC director axis (which is typically the extraordinary axis) rotates through an angle from the input to the output surface, commonly known as the twist angle. The retardance can be tuned via an applied voltage that causes the LC director axis to tilt. Recently, TN-LC components have also received considerable interest for manufacturing broadband retarders with improved properties using multi-twist stacks [2]. The twisted retarder structure is very interesting as a polarization transforming device because it can be regarded as a combination of effective linear retardance and effective optical rotation (circular retardance).

Different methods were developed in the past to describe the polarization properties of twisted anisotropic media [3], including the early works of R. C. Jones [4]. Because of the interest of using TN-LC modulators as phase-only spatial light modulators (SLM), Lu and Saleh [5] extended these Jones matrices by introducing the optical modulation assuming a voltage-dependent effective extraordinary refractive index $n_{ef}(V)$, thus leading to a variable retardance $\beta(V)$. After this seminal work, different approaches aimed at predicting the optical modulation with higher accuracy were proposed. Such refined models considered the LC edge layers coated to the device surfaces, where the LC director is unable to tilt freely as it does in the center of the LC cell, therefore adding a second retardance parameter $\delta(V)$ [6–8].

The analytical Jones matrices used in these previous works are expressed in a reference framework where the LC director at the input surface of the modulator is aligned with the x-axis. Therefore, the proper application of these models requires a prior precise determination of the twist angle (α) and the LC orientation (ψ_D). This orientation cannot be measured directly as in the standard case of a linear retarder, where the neutral axes can be found simply by looking for maximum light extinction between crossed polarizers. Instead, techniques using different wavelengths or spectroscopic procedures have been applied, where the spectral dependence of the maximum retardance ($\beta_{max}(\lambda)$)

* Corresponding author.
E-mail address: i.moreno@umh.es (I. Moreno).

https://doi.org/10.1016/j.optlastec.2022.108567
Received 12 August 2021; Received in revised form 29 July 2022; Accepted 1 August 2022

provides sufficient information to solve possible ambiguities [9,10]. Other approaches are based on a single wavelength characterization and measurements with different polarization configurations [11,12]. All these techniques typically retrieve the LC parameters by simultaneously fitting a set of experimental curves to numerical values of ψ_D, α and β_{max}. Because ψ_D and α are fixed parameters, and $\beta_{max}(\lambda)$ can be interpolated using standard dispersion relations, the spectral modulation can be derived out of measurements made at sample wavelengths [13]. Additional experiments are required to univocally determine the sense of rotation of the LC director (sign of α) and to distinguish between the extraordinary and ordinary LC axes [14]. These techniques were proved successful in the characterization of TN-LC cells. However, their application requires performing several measurements and the simultaneous fitting of the microscopic physical parameters ψ_D, α and β_{max} to numerical data. To avoid such cumbersome calibration procedures, other approaches avoid any assumption on the LC microscopic physical model and directly measure the Jones matrix [15,16], or an equivalent retarder-rotator system [17].

Another standard mathematical description of polarization is the Mueller-Stokes (MS) approach [18]. Within this formalism, polarization states are described by the four Stokes parameters and polarization devices are described by 4x4 Mueller matrices. Some works used the MS formalism to describe TN-LCDs [19–22] since it provides a more complete polarimetric description, including parameters like depolarization, diattenuation and polarizance. The MS approach became especially relevant when liquid–crystal on silicon (LCOS) technology [23] emerged. In these devices the phase fluctuations originated by flicker can result in an effective depolarization [24] that cannot be measured in the Jones matrix approach. Hence, Mueller-matrix polarimetry has become a standard technique for characterizing polarization components and devices, including TN-LC modulators. However, the works that apply the MS approach do not generally consider a physical model for the TN-LC cell; they are based instead on empirical polarization measurements. This implies that the TN modulator must be fully calibrated for each wavelength of interest. In addition, the MS approach does not account for phase modulation, and therefore a combined approach is required to fully predict the complex optical modulation [25].

In the last decade, LCOS devices with vertically-aligned (VAN) or zero-twist electrically controlled birefringence (ECB) configurations became the dominant technology for phase-only SLMs [23]. Even though TN-LC SLMs proved to be very effective as phase-only SLMs with properly adjusted polarization configurations [26–29], they have generally been abandoned for this purpose, mainly due to the complex and time-consuming techniques required to achieve these phase-only configurations. They could not compete with the ease of configuring VAN/ECB LC devices, which only require finding the direction of the principal axes and aligning the input linear polarization parallel to the modulating axis. Regardless, TN-LC SLMs remain more affordable as compared to the costly VAN/ECB LCOS devices.

In this work we consider a physical model of the TN-LC cell and perform a complete Mueller matrix polarimetric analysis to fully characterize its physical parameters and its optical modulation. We first review the analytical Jones matrices describing the physical model of the TN-LC modulator and derive the corresponding Mueller matrices in the different modulation regimes. We show that a MS polarimetric analysis allows to characterize the physical parameters of the TN-LC cell. For instance, α can easily be determined when the TN-LC acts as a pure polarization rotator, while the polarization eigenstates give a direct measurement of ψ_D, thus enabling an independent single wavelength measurement of these two parameters. The Mueller matrix further provides an unambiguous distinction between the fast and slow axes, and the sense of rotation of the LC director. Then, we identify the elements of the Mueller matrix that yield a full characterization of the TN-LC optical modulation retardances $\beta(V)$ and $\delta(V)$ related, respectively, to the central and edge LC layers in the cell [5,7]. These procedures provide a complete description of the modulation properties. Finally, based on the assumption that the TN-LC is a pure retarder component, a simplified method is presented at the end of the paper. This simplified characterization requires fewer measurements than the full Mueller matrix characterization, thus enabling a rapid configuration of the modulator in the laboratory.

The paper is organized as follows. After this introduction, Section 2 reviews the Jones matrix and the Mueller matrix describing the TN-LC cell, and the description of its polarization eigenstates and retardance vector. Then, Section 3 shows the experimental Mueller matrix characterization, including the location of the pure polarization rotator regime, and how this can be used to completely determine the device physical parameters and its optical modulation. Section 4 develops the simplified procedure, valid under the assumption of a pure retarder device, which is shown to yield equivalent results. Finally, Section 5 gives the conclusions.

2. Review of the TN-LC cell and its modulation regimes

In this section we review the polarization transformations induced by a TN-LC cell. At this point we consider the model by Lu and Saleh [5].

2.1. Jones matrix for the TN-LC cell

According to this model, the Jones matrix of a TN-LC cell where the LC director axis of the first layer is assumed to be aligned along the x-axis of the coordinate system, reads

$$\mathbf{M}_{\mathbf{TNLC}} = e^{-i\beta}\mathbf{R}(-\alpha)\cdot\mathbf{M}(X,Y,Z), \tag{1}$$

where $\mathbf{R}(-\alpha)$ is the 2×2 rotation matrix (we follow the notations by Saleh and Teich in [30]):

$$\mathbf{R}(\alpha) = \begin{bmatrix} \cos\alpha & \sin\alpha \\ -\sin\alpha & \cos\alpha \end{bmatrix}, \tag{2}$$

and $\mathbf{M}(X,Y,Z)$ is given by [13]:

$$\mathbf{M}(X,Y,Z) = \begin{bmatrix} X-iY & Z \\ -Z & X+iY \end{bmatrix}, \tag{3}$$

with the restriction $X^2+Y^2+Z^2=1$. After symmetry considerations, the matrix decomposition in Eqs. (1)–(3) was demonstrated to be the general expression for any TN-LC cell, independent of the specific distribution of the twist and tilt angle along the cell [31]. Therefore, we will henceforth use the X,Y,Z functions.

In the standard model by Lu and Saleh [5], X,Y,Z depend on the twist angle α and on the LC retardance $2\beta = (2\pi/\lambda)\Delta n\cdot t$ (here λ denotes the wavelength, $\Delta n = n_e - n_o$ is the birefringence of the LC material, and t is the thickness of the LC layer) as.

$$X = \cos\gamma,\ Y = \frac{\beta}{\gamma}\sin\gamma,\ Z = \frac{\alpha}{\gamma}\sin\gamma, \tag{4}$$

where $\gamma = \sqrt{\alpha^2+\beta^2}$. This model provides a very accurate description of the TN-LC cell in the absence of applied voltage.

Upon applying a voltage to the modulator, the LC tilts an angle $\theta(V)$ in the central region of the LC cell. The standard Lu and Saleh model [5] considers the optical modulation driven by the voltage-dependent retardance parameter $\beta(V)$ which now depends on the tilt angle as

$$\beta(V) = \frac{\pi}{\lambda}\left[n_{ef}(\theta(V)) - n_o\right]\cdot t, \tag{5}$$

where the effective extraordinary index n_{ef} is related to the LC tilt angle θ by.

$$\frac{1}{n_{ef}^2(\theta)} = \frac{\sin^2(\theta)}{n_o^2} + \frac{\cos^2(\theta)}{n_e^2}. \tag{6}$$

By changing the value of parameter β in Eq. (5) three interesting regimes can be found:

(a) The *adiabatic regime* [3], also named *Maugin limit* [32], which is achieved when $\beta \gg \alpha$, and therefore $\gamma \simeq \beta$, so the matrix in Eq. (1) can be approximated as:

$$\mathbf{M_{TNLC}}(\beta \gg \alpha) = e^{-i\beta}\mathbf{R}(-\alpha)\cdot\begin{bmatrix} e^{-i\beta} & 0 \\ 0 & e^{+i\beta} \end{bmatrix}, \tag{7a}$$

i.e., the TN-LC cell behaves as a combination of a polarization rotator and linear retarder.

(b) When $\gamma = m\pi$ (m being an integer number) the device becomes a pure polarization rotator since the Jones matrix $\mathbf{M}$ in Eq. (3) becomes the identity matrix, i.e.:

$$\mathbf{M_{TNLC}}(\gamma = m\pi) = e^{-i\beta}\mathbf{R}(-\alpha)(-1)^m. \tag{7b}$$

This situation is known as the *Gooch-Tarry relation* [32] or as a *local adiabatic point* [33].

(c) (Finally, in the limit of low birefringence $\beta \to 0$ we find that $\gamma \to \alpha$ and the matrix $\mathbf{M}$ in Eq. (3) becomes a rotation matrix $\mathbf{R}(+\alpha)$ that cancels $\mathbf{R}(-\alpha)$ in Eq. (1), so the global TN-LC Jones matrix becomes the identity matrix $\mathbf{M_{TNLC}}(\beta \to 0) = \mathbf{I}$.

In TN-LC modulators the twist angle is typically $\alpha = \pm\pi/2$ and the birefringence parameter varies between the limit $\beta = 0$ and at least the first adiabatic point, $\gamma = \pi$. In such case the Jones matrix changes from being the identity matrix, thus not changing the input polarization, to become a pure rotator matrix $\mathbf{R}(-\alpha)$, thus rotating the input polarization by the twist angle.

Finally, let us emphasize that this form of the Jones matrix in Eq. (1) is valid provided the LC director at the input surface of the modulator is aligned along the x-coordinate axis of the reference framework. In case the LC director forms an angle ψ_D with the x-axis, the Jones matrix must be calculated using the standard rotation transformation given by [30]:

$$\mathbf{M_{TNLC}}(\psi_D) = \mathbf{R}(-\psi_D)\cdot\mathbf{M_{TNLC}}\cdot\mathbf{R}(+\psi_D). \tag{8}$$

2.2. Mueller matrix for the TN-LC cell

The previous section provides an analytical description of the TN-LC cell within the Jones matrix formalism. However, the MS formalism allows to obtain additional polarimetric information. The Mueller matrix $\widetilde{\mathbf{M}}$ of a pure retarder can be calculated from the corresponding Jones matrix $\mathbf{M}$ as [18]:

$$\widetilde{\mathbf{M}} = \mathbf{A}\cdot(\mathbf{M}\otimes\mathbf{M})\cdot\mathbf{A}^{-1}, \tag{9}$$

where $\otimes$ denotes the tensor (Kronecker) product and where

$$\mathbf{A} = \begin{bmatrix} 1 & 0 & 0 & 1 \\ 1 & 0 & 0 & -1 \\ 0 & 1 & 1 & 0 \\ 0 & i & -i & 0 \end{bmatrix}. \tag{10}$$

Alternatively, the elements m_{ij} of the Mueller matrix ($i,j = 0,1,2,3$) can be obtained as [18]:

$$m_{ij} = \frac{1}{2}\mathrm{Tr}\left(\mathbf{M}\cdot\sigma_i\cdot\mathbf{M}^{+}\cdot\sigma_j\right), \tag{11}$$

where $\mathrm{Tr}(\bullet)$ denotes the trace of the matrix, $+$ the Hermitian conjugate and σ are the set of four 2×2 matrices comprising the identity matrix and the Pauli matrices, i.e.

$$\sigma_0 = \begin{pmatrix} 1 & 0 \\ 0 & 1 \end{pmatrix}, \sigma_1 = \begin{pmatrix} 1 & 0 \\ 0 & -1 \end{pmatrix}, \sigma_2 = \begin{pmatrix} 0 & 1 \\ 1 & 0 \end{pmatrix}, \sigma_3 = \begin{pmatrix} 0 & -i \\ i & 0 \end{pmatrix} \tag{12}$$

For the case of a pure retarder element (i.e., an element without diattenuation, polarizance or depolarization) the Mueller matrix takes the form:

$$\widetilde{\mathbf{M}}_R = \begin{bmatrix} 1 & \overrightarrow{0} \\ \overrightarrow{0}^T & \widetilde{\mathbf{m}}_R \end{bmatrix}, \tag{13}$$

where $\overrightarrow{0} = (0,0,0)$ and $\widetilde{\mathbf{m}}_R$ is a 3×3 real unitary matrix. In this section we consider ideal TN-LC cells that are pure retarder elements described by the Jones matrix in Eqs. (1)–(3). Therefore, the corresponding Mueller matrix can be described only by submatrix $\widetilde{\mathbf{m}}_R$.

Considering Eqs. (1), (9)–(12), the Mueller submatrix $\widetilde{\mathbf{m}}_{\mathrm{TNLC}}$ describing the TN-LC cell results in an equivalent product $\widetilde{\mathbf{m}}_{\mathrm{TNLC}} = \widetilde{\mathbf{R}}(-\alpha)\bullet\widetilde{\mathbf{m}}$, where the rotation matrix $\widetilde{\mathbf{R}}(\alpha)$ and the matrix $\widetilde{\mathbf{m}}$ now in the Mueller formalism read:

$$\widetilde{\mathbf{m}}_{\mathrm{TNLC}} = \widetilde{\mathbf{R}}(-\alpha)\cdot\widetilde{\mathbf{m}} =$$

$$= \begin{bmatrix} \cos(2\alpha) & \sin(2\alpha) & 0 \\ -\sin(2\alpha) & \cos(2\alpha) & 0 \\ 0 & 0 & 1 \end{bmatrix}\cdot\begin{bmatrix} 1-2Z^2 & 2XZ & -2YZ \\ -2XZ & 2X^2-1 & -2XY \\ -2YZ & 2XY & 1-2Y^2 \end{bmatrix}. \tag{14}$$

The adiabatic regime achieved when $\beta \gg \alpha$ (or equivalently $\gamma \simeq \beta$) (Eq. (7a)) results in:

$$\widetilde{\mathbf{m}}_{\mathrm{TNLC}}(\beta \gg \alpha) = \widetilde{\mathbf{R}}(-\alpha)\cdot\begin{bmatrix} 1 & 0 & 0 \\ 0 & \cos(2\beta) & -\sin(2\beta) \\ 0 & \sin(2\beta) & \cos(2\beta) \end{bmatrix}. \tag{15}$$

Similarly, the pure rotator regime achieved when $\gamma = \pi$ (Eq. (7b)) leads to the Mueller matrix $\widetilde{\mathbf{m}}_{\mathrm{TNLC}}(\gamma = \pi) = \widetilde{\mathbf{R}}(-\alpha)$, and the limit $\beta \to 0$ results in an identity Mueller matrix.

The matrix product $\widetilde{\mathbf{m}}_{\mathrm{TNLC}} = \widetilde{\mathbf{R}}(-\alpha)\cdot\widetilde{\mathbf{m}}$ n Eq. (14) results in.

$$\widetilde{\mathbf{m}}_{\mathrm{TNLC}} = \begin{bmatrix} 2XZs + (1-2Z^2)c & 2XZc + (2X^2-1)s & 2XYs - 2YZc \\ (1-2Z^2)s - 2XZc & (2X^2-1)c + 2XZs & -2XYc - 2YZs \\ -2YZ & 2XY & 1-2Y^2 \end{bmatrix} \tag{16}$$

where $s = \sin(2\alpha)$ and $c = \cos(2\alpha)$. For the standard twist angle $\alpha = \pm\pi/2$ it results in:

$$\widetilde{\mathbf{m}}_{\mathrm{TNLC}} = \begin{bmatrix} 2Z^2-1 & -2XZ & 2YZ \\ 2XZ & 1-2X^2 & 2XY \\ -2YZ & 2XY & 1-2Y^2 \end{bmatrix}. \tag{17}$$

Finally, like in the Jones formalism, the Mueller matrix in Eq. (14)-(17) is valid provided the LC director at the input surface of the modulator is aligned with the x-axis of the reference framework. In case it is rotated by an angle ψ_D the corresponding Mueller matrix is calculated as $\widetilde{\mathbf{m}}_{\mathrm{TNLC}}(\psi_D) = \widetilde{\mathbf{R}}(-\psi_D)\cdot\widetilde{\mathbf{m}}_{\mathrm{TNLC}}\cdot\widetilde{\mathbf{R}}(+\psi_D)$.

Table 1 summarizes the Jones and the Mueller matrices for the different regimes of the TN-LC cell, as well as the general case for the standard twist angle $\alpha = \pm\pi/2$.

Fig. 1(a) illustrates the variation of the X, Y, Z functions in the Lu and Saleh model [5] (Eqs. (4) and (5)) represented versus the retardance parameter β for a TN-LC cell with $\alpha = +\pi/2$. The horizontal axis is displayed in inverse sense to better compare with the experimental results presented in the next section. Note that for $\beta = \sqrt{3}\pi/2 = 0.866\pi$ the first pure rotator (local adiabatic) point is reached. This is marked with a vertical line in the graph, noting that $Y = Z = 0$ and $X = -1$ at this point. Fig. 1(b) shows the corresponding elements m_{ij} ($i,j = 1,2,3$) of the Mueller submatrix as a function of β, again for a TN-LC cell with $\alpha = +\pi/2$. These curves also illustrate the transition from the identity matrix ($\beta = 0$) to the pure rotation matrix achieved when $\beta = 0.866\pi$, where $m_{11} = m_{22} = -1$ and $m_{33} = +1$ and all the rest of elements vanish. Let us highlight the large variation of the element m_{22}, which changes from $+1$ to -1 and back to $+1$. For a TN-LC cell with $\alpha = \pi/2$ the Lu

Table 1
Jones and Mueller matrices for different regimes of the TNLC cell.

Regime	Jones matrix $\mathbf{M}_{\mathrm{TNLC}}$	Mueller submatrix $\widetilde{\mathbf{m}}_{\mathrm{TNLC}}$
General case	$e^{-i\beta}\mathbf{R}(-\alpha)\cdot\begin{bmatrix} X-iY & Z \\ -Z & X+iY \end{bmatrix}$	$\widetilde{\mathbf{R}}(-\alpha)\cdot\begin{bmatrix} 1-2Z^2 & 2XZ & -2YZ \\ -2XZ & 2X^2-1 & -2XY \\ -2YZ & 2XY & 1-2Y^2 \end{bmatrix}$
Adiabatic limit ($\beta \gg \alpha$)	$e^{-i\beta}\mathbf{R}(-\alpha)\cdot\begin{bmatrix} \exp(-i\beta) & 0 \\ 0 & \exp(i\beta) \end{bmatrix}$	$\widetilde{\mathbf{R}}(-\alpha)\cdot\begin{bmatrix} 1 & 0 & 0 \\ 0 & \cos(2\beta) & -\sin(2\beta) \\ 0 & \sin(2\beta) & \cos(2\beta) \end{bmatrix}$
First pure rotator point ($\gamma = \pi$)	$-e^{-i\beta}\begin{bmatrix} \cos(\alpha) & -\sin(\alpha) \\ \sin(\alpha) & \cos(\alpha) \end{bmatrix}$	$\begin{bmatrix} \cos(2\alpha) & -\sin(2\alpha) & 0 \\ \sin(2\alpha) & \cos(2\alpha) & 0 \\ 0 & 0 & 1 \end{bmatrix}$
General case with standard twist $\alpha = \pi/2$	$e^{-i\beta}\begin{bmatrix} Z & -X-iY \\ X-iY & Z \end{bmatrix}$	$\begin{bmatrix} 2Z^2-1 & -2XZ & 2YZ \\ 2XZ & 1-2X^2 & 2XY \\ -2YZ & 2XY & 1-2Y^2 \end{bmatrix}$

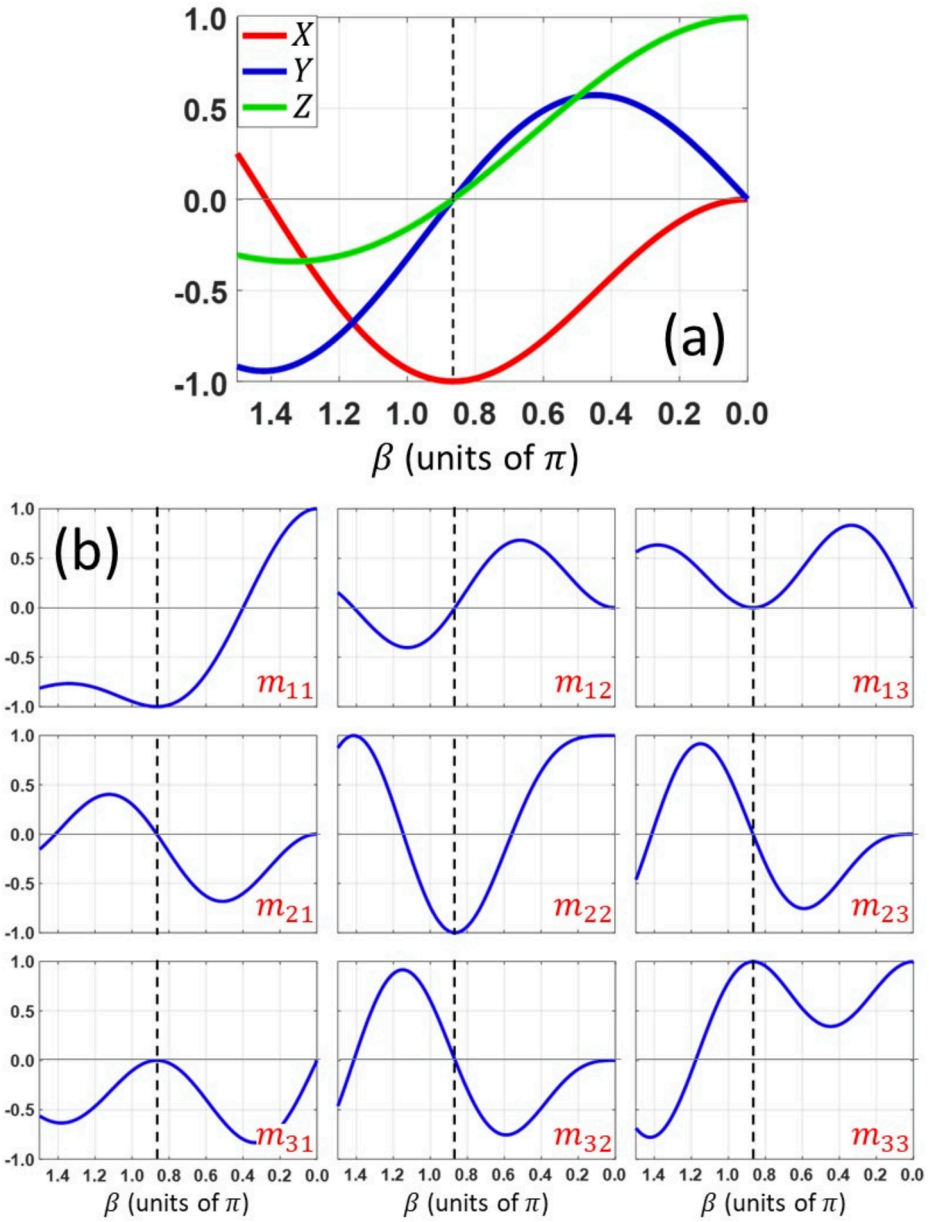

Fig. 1. (a) Evolution of the X, Y, Z functions with respect to β for a TN-LC cell with $\alpha = +\pi/2$ in the Lu and Saleh model [5]. (b) m_{ij} elements of the corresponding Mueller submatrix. The pure rotator (local adiabatic point) is found at $\beta = 0.866\pi$ (marked with a vertical line).

and Saleh model [5] leads to the relation $m_{22} = 1 - 2X^2 = -\cos(2\gamma)$. The large variation of m_{22} makes it ideal for an accurate measurement of γ_{max}, and consequently of $\beta_{max} = \sqrt{\gamma_{max}^2 - \alpha^2}$.

The normalized transmission of the TN-LC cell between linear polarizers (T_L) can be calculated using either the Jones matrix or the Mueller matrix. If the input and output polarizers have orientations ξ_1 and ξ_2 relative to the LC director at the input surface ($x-$ axis), the normalized transmission is given by the relation.

$$T_L(\xi_1,\xi_2) = \left(X\cos(\xi_1 - \xi_2 + \alpha) + Z\sin(\xi_1 - \xi_2 + \alpha)\right)^2 + \left(Y\cos(\xi_1 + \xi_2 - \alpha)\right)^2 \quad (18)$$

while when the TN-LC cell is inserted between circular polarizers, it is given by.

$$T_{C\perp} = Y^2 \text{ and } T_{C\parallel} = X^2 + Z^2 \quad (19)$$

where $T_{C\perp}$ and $T_{C\parallel}$ denote respectively the transmission for crossed and parallel circular polarizers. Note that the relations in Eq. (19) are independent of the TN-LC cell orientation, i.e., independent of ψ_D, thus being useful to find the adiabatic point even without knowing the correct orientation.

2.3. Retardance vector and polarization eigenstates

Retarders can be characterized by the retardance vector $\vec{\mathbf{R}}$ [34–36], whose magnitude R is given by the total retardance, which is obtained from the Mueller matrix as.

$$\cos(R) = \frac{1}{2}\mathrm{Tr}[\widetilde{\mathbf{M}}_R] - 1 = \frac{1}{2}\mathrm{Tr}[\widetilde{\mathbf{m}}_R] - \frac{1}{2}, \quad (20)$$

and whose components can be calculated as.

$$\vec{\mathbf{R}} = R\widehat{\mathrm{R}} = \begin{bmatrix} R_H \\ R_{45} \\ R_C \end{bmatrix} = R\frac{1}{2\sin(R)}\begin{bmatrix} m_{R23} - m_{R32} \\ m_{R31} - m_{R13} \\ m_{R12} - m_{R21} \end{bmatrix}, \quad (21)$$

where $R_L = \sqrt{R_H^2 + R_{45}^2}$ is the total linear retardance and R_C the circular retardance. Alternatively, an equivalent approach can be applied within the Jones formalism for instance by applying the parametrization by Arteaga and Canillas [37].

The application of Eqs. (20)–(21) to the Mueller matrix in Eq. (16) allows obtaining analytical expressions for the retardance vector in terms of the X, Y, Z functions describing the TN-LC cell. The total retardance is given by.

$$\cos(R) = \left(X^2 - Z^2\right)\cos(2\alpha) + 2XZ\sin(2\alpha) - Y^2, \quad (22)$$

which can be reduced to

$$\cos\left(\frac{R}{2}\right) = X\cos(\alpha) + Z\sin(\alpha), \quad (23)$$

and the retardance vector is

$$\vec{\mathbf{R}} = \frac{R}{\sin R}\begin{bmatrix} -XY(1+\cos(2\alpha)) - YZ\sin(2\alpha) \\ -YZ(1-\cos(2\alpha)) - XY\sin(2\alpha) \\ 2XZ\cos(2\alpha) - 2\left(X^2 - Z^2\right)\sin(2\alpha) \end{bmatrix}. \quad (24)$$

For the standard twist angle $\alpha = \pi/2$, then $\cos(R/2) = Z$ and the retardance vector reduces to

$$\vec{\mathbf{R}} = R\frac{1}{\sqrt{X^2 + Y^2}}\begin{bmatrix} 0 \\ -Y \\ -X \end{bmatrix}, \quad (25)$$

so the linear and circular retardances are given by $R_H = 0$, $R_{45}/R = -Y/\left(\sqrt{X^2 + Y^2}\right)$ and $R_C/R = -X/\left(\sqrt{X^2 + Y^2}\right)$. Let us emphasize that these retardances are effective parameters. The liquid–crystal layer is a linear retarder, but its twisted structure generates the effective circular retardance. Fig. 2(a) illustrates the evolution of R,R_L and R_C as a function of β for the standard case of a twist $\alpha = \pi/2$. The special value $\beta = 0.866\pi$ corresponding to the first local adiabatic point is again marked to highlight that at this value, the cell behaves as a pure polarization rotator, and therefore it only exhibits circular retardance.

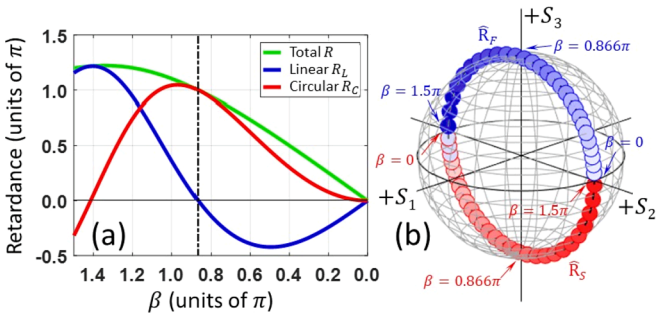

Fig. 2. (a) Total, linear and circular retardances of a TN-LC cell with $\alpha = +\pi/2$ with respect to β. The pure rotator (local adiabatic point) is found at $\beta = 0.866\pi$. (b) Evolution in the Poincaré sphere of the polarization eigenstates $\widehat{\mathrm{R}}_F$ (blue dots) and $\widehat{\mathrm{R}}_S$ (red dots) of $\mathbf{M}_{\mathbf{TNLC}}$. (For interpretation of the references to colour in this figure legend, the reader is referred to the web version of this article.)

The normalized vector $\widehat{\mathrm{R}}_F = \vec{\mathbf{R}}/R$ provides the Stokes parameters $\widehat{\mathrm{R}}_F = (S_1, S_2, S_3)^T$ of the fast polarization eigenstate of the equivalent elliptical retarder, while the orthogonal state $\widehat{\mathrm{R}}_S = -\widehat{\mathrm{R}}_F$ is the slow polarization eigenstate. The eigenstates $\widehat{\mathrm{R}}_F$ and $\widehat{\mathrm{R}}_S$ are polarization states that are transmitted though the TN-LC cell without changing its polarization, simply gaining a phase. This concept was employed for the configuration of the TN-LC modulators as phase-only SLMs devices [26]. The orientation (ψ) and ellipticity (ε) angles of the eigenvectors are given by their Stokes parameters as $\tan(2\psi) = S_2/S_1$ and $\tan(2\varepsilon) = S_3/\sqrt{S_1^2 + S_2^2}$ [18]. Therefore, from Eq. (25), the fast eigenstate of the TN-LC cell has an azimuth angle given by.

$$\tan(2\psi) = \frac{Z(1-\cos(2\alpha)) + X\sin(2\alpha)}{X(1+\cos(2\alpha)) + Z\sin(2\alpha)}. \quad (26)$$

Using simple trigonometric relations, this equation can be simplified to $\tan(2\psi) = \tan(\alpha)$, which shows that the orientation of the polarization eigenstate is constant, equal to $\psi = \alpha/2$. For the standard twist $\alpha = \pi/2$, $\widehat{\mathrm{R}}_F$ is oriented at $\psi = \pi/4$ while its ellipticity changes as $2\varepsilon = \arctan(X/Y)$. In this derivation we used the Mueller matrix (Eq. (14)-(16)) for a TN cell with the LC director at the input surface parallel to the x-axis. Therefore, the eigenstate azimuth constant value $\psi = \alpha/2$ is relative to the x-axis. This angle is useful to locate the orientation of the LC director in the laboratory frame reference once α is known, i.e., it allows determining the angle ψ_D.

Fig. 2(b) illustrates the evolution of the fast and slow eigenstates as a function of β, again for the standard case of twist angle $\alpha = +\pi/2$ and for a variation in the range $\beta \in [0, 1.5\pi]$. As expected from the previous discussion, these states are aligned along the meridian in the plane $S_2 - S_3$ of the Poincaré sphere while the ellipticity changes with β. At the local adiabatic point, where the TN-LC cell becomes a pure polarization rotator, the eigenstates become circularly polarized.

3. Experimental Mueller matrix polarimetric characterization

In this section we experimentally verify the former predictions by using a standard Mueller matrix polarimeter, with a polarization state generator (PSG) composed of a linear polarizer and a quarter-wave plate (QWP), and a polarization state analyzer (PSA) composed by a second

QWP and a second polarizer. We use the standard polarization states (linear states horizontal, vertical and at $\pm 45^{\circ}$, and circular R and L states), both in the PSG and in the PSA. A He-Ne laser (Melles Griot, 25-LHP-151–230) of 632.8 nm wavelength is used. In the experiments we consider the x-axis aligned along the horizontal direction in the laboratory, and we measure positive angles as counterclockwise rotated from the analyzer point of view.

We tested a 2 cm diameter circular single cell TN-LC modulator

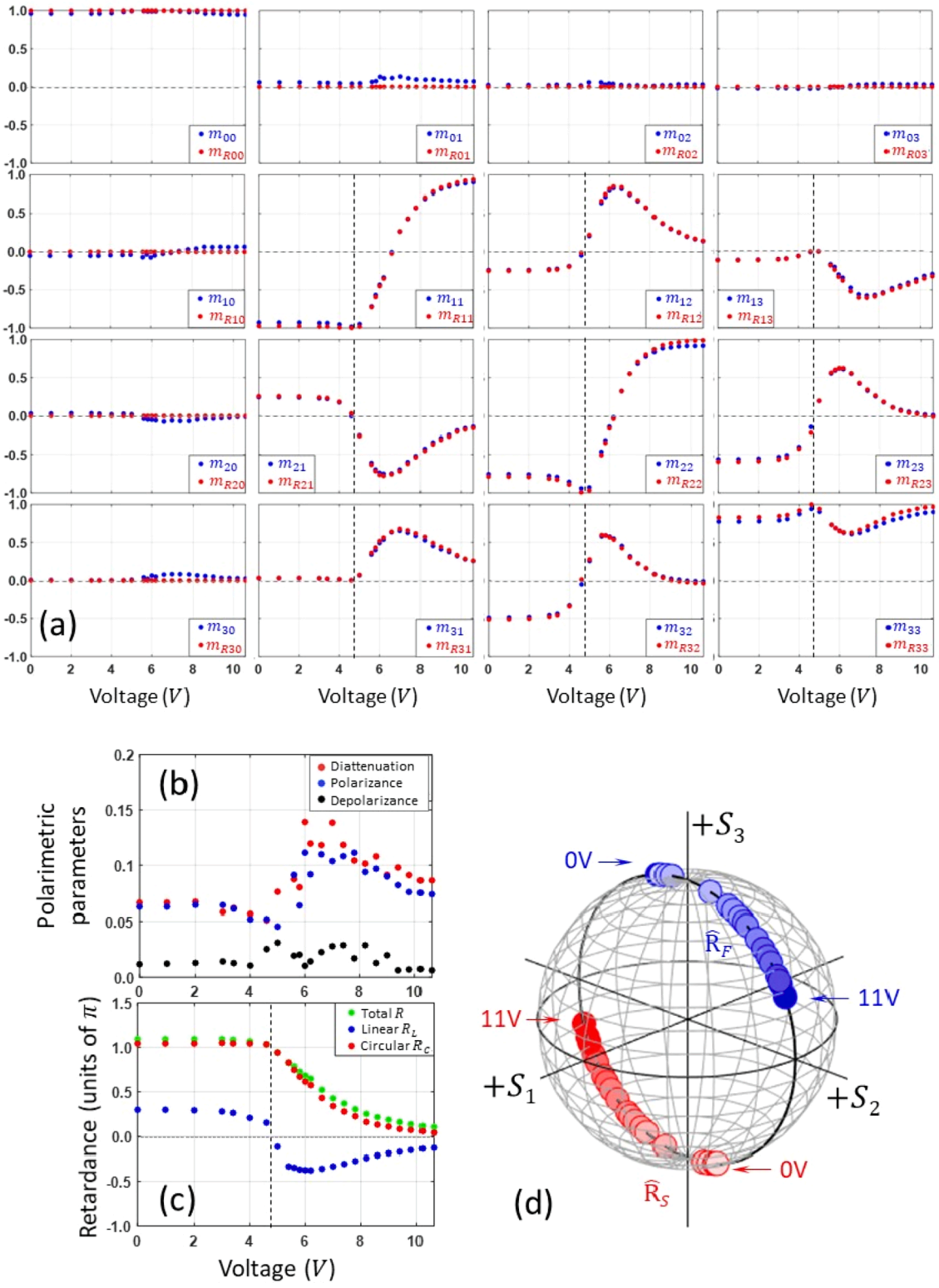

Fig. 3. (a) Experimental measurement of the Mueller matrix elements for the TN-LC modulator as a function of the applied voltage (blue dots) and the corresponding retarder matrix derived from the Lu -Chipman decomposition (red dots). (b) Diattenuation, polarizance and depolarizance. (c) Total, linear and circular retardances. (d) Polarization eigenstates of the retarder represented in the Poincaré sphere. (For interpretation of the references to colour in this figure legend, the reader is referred to the web version of this article.)

(Jenoptic, model ALM) that is driven by a wavefunction generator, which addresses a 2 kHz square DC balanced electrical signal of peak-to-peak voltage (Vpp) ranging from zero to 11 V. The Mueller matrix is calibrated for each Vpp value. Fig. 3(a) shows the 16 elements of the measured matrix and their evolution with Vpp (blue dots). All curves were normalized to the maximum value of m_{00} measured for the complete voltage range. The results are close to those expected for a pure retarder element, i.e., with $m_{00} = 1$, $m_{i0} = 0$ and $m_{0j} = 0$ $(i,j = 1,2,3)$. However, non-negligible variations are observed in the elements of the first row and first column. Therefore, we applied the Lu-Chipman polar decomposition [35], which expresses the measured Mueller matrix as $\widetilde{\mathbf{M}} = \widetilde{\mathbf{M}}_\Delta \cdot \widetilde{\mathbf{M}}_R \cdot \widetilde{\mathbf{M}}_D$ where $\widetilde{\mathbf{M}}_D$,$\widetilde{\mathbf{M}}_R$ and $\widetilde{\mathbf{M}}_\Delta$ are the diattenuator, retarder and depolarizer matrix components. The polarizance and diattenuation values in Fig. 3(b) are comprised below 0.15 in the complete range, and the depolarizance remains below 0.05.

Fig. 3(a) also shows (red dots) the retarder matrix $\widetilde{\mathbf{M}}_R$ obtained within the Lu-Chipman polar decomposition. These curves are very close to those of $\widetilde{\mathbf{M}}$. The curves show no variation for Vpp between zero and 3 V, since the threshold voltage to induce LC molecular tilt is not reached yet. In the other extreme, for voltages above 10 Vpp the matrix approaches the identity matrix (limit $\beta \to 0$). In between, large variations are observed in the elements of the 3×3 submatrix $\widetilde{\mathbf{m}}_R$, which follow a behavior like the simulation in Fig. 2(a) for values of β in the range $[1.1\pi, 0]$.

At Vpp = 4.6 V, the effective linear retardance goes to zero, and all the retardance becomes circular. At this voltage, the TN-LC cells is in the first adiabatic point and behaves as a pure polarization rotator. Therefore, the rotation angle for input linearly polarized light at this point directly provides a direct measurement of the twist angle. In our device we measured a rotation of $90° \pm 1°$, where the uncertainty comes from the minimum scale we can measure in the rotating mount of the polarizer. In fact, since the rotation is related to the circular retardance as $\alpha = R_C/2$, the value $R_C = \pi$ measured at Vpp = 4.6 V confirms the twist angle $\alpha = \pi/2$.

A second useful result is shown in Fig. 3(d). The retardance vector is calculated using Eqs. (20) and (21) and its components provide the effective linear and circular retardances, as shown in Fig. 3(c). The normalized vectors $\widehat{\mathrm{R}}_F$ and $\widehat{\mathrm{R}}_S$ related to the fast and slow eigenstates are shown in Fig. 3(d) represented on the Poincaré sphere. Note that the eigenstates are oriented along the $S_2 - S_3$ plane, as expected from the discussion of Fig. 2. This confirms that the TN-LC cell was correctly aligned with respect to the laboratory x-axis ($\psi_D = 0$). If the TN-LC cell had not been correctly oriented ($\psi_D \neq 0$) these eigenstates would appear aligned along another meridian of the Poincaré sphere, oriented at an azimuth $\psi = \pi/4 + \psi_D$.

Since the TN-LC cell is oriented with the LC director parallel to the x-axis of the laboratory framework ($\psi_D = 0$), the measured Mueller matrix elements in Fig. 3(a) follow a qualitative behavior like Eq. (17). In this situation the Mueller matrix measurement also resolves two remaining ambiguities. The sign of α indicates the rotation sense of the LC director inside the cell, while the change in ψ_D to $\psi_D + \pi/2$ exchanges the orientation of the extraordinary and ordinary axes. Since the extraordinary axis depends on the applied voltage, this ambiguity was traditionally resolved by means of additional experiments that depend on the phase modulation [13,14]. However, these ambiguities can be easily resolved from the data in Fig. 3, for instance, by noting the variations on the m_{12} and m_{13} Mueller matrix elements. Fig. 4 shows a simulation of the four situations that may occur. Changing the sign of α inverts also the sign of both m_{12} and m_{13} elements. On the contrary, changing $\psi_D \to \psi_D + \pi/2$ inverts the sign of the element m_{13}, while leaving m_{12} unaltered. Therefore, according to the experimental result in Fig. 3 (a) one can conclude the positive sense of the twist angle in our device and the value $\psi_D = 0$, thus indicating that the $x-$ axis of the laboratory coincides with the LC director at the input face of the LC cell.

Finally, it is also interesting to obtain the retardances modulation parameters related to the microscopic description of the TN-LC cell. Here we use the Lu & Saleh model [5] that considers the retardance parameter $\beta(V)$, corrected by the edge LC layers [7] by means of a second retardance parameter $\delta(V)$. For this refined model, the X, Y functions in Eq. (4) must be modified to.

$$X = \cos(\gamma)\cos(2\delta) - \frac{\beta}{\gamma}\sin(\gamma)\sin(2\delta), \tag{27a}$$

$$Y = \cos(\gamma)\sin(2\delta) + \frac{\beta}{\gamma}\sin(\gamma)\cos(2\delta), \tag{27b}$$

while Z is insensitive to the edge layers. The diagonal elements of the Mueller matrix for the twist angle $\alpha = \pm\pi/2$ [Eq. (17)] provide a direct measurement of the X, Y, Z functions as:

$$X = \sqrt{\frac{1}{2}(1 - m_{22})},\ Y = \sqrt{\frac{1}{2}(1 - m_{33})},\quad Z = \sqrt{\frac{1}{2}(1 + m_{11})} \tag{28}$$

In case the twist angle was different, a similar calculation could be obtained from Eq. (16) once the matrix product $\widetilde{\mathbf{m}} = \widetilde{\mathbf{R}}(+\alpha)\cdot\widetilde{\mathbf{m}}_{\mathrm{TNLC}}$ is calculated.

Fig. 5(a) shows the functions $X(V)$, $Y(V)$ and $Z(V)$ calculated from

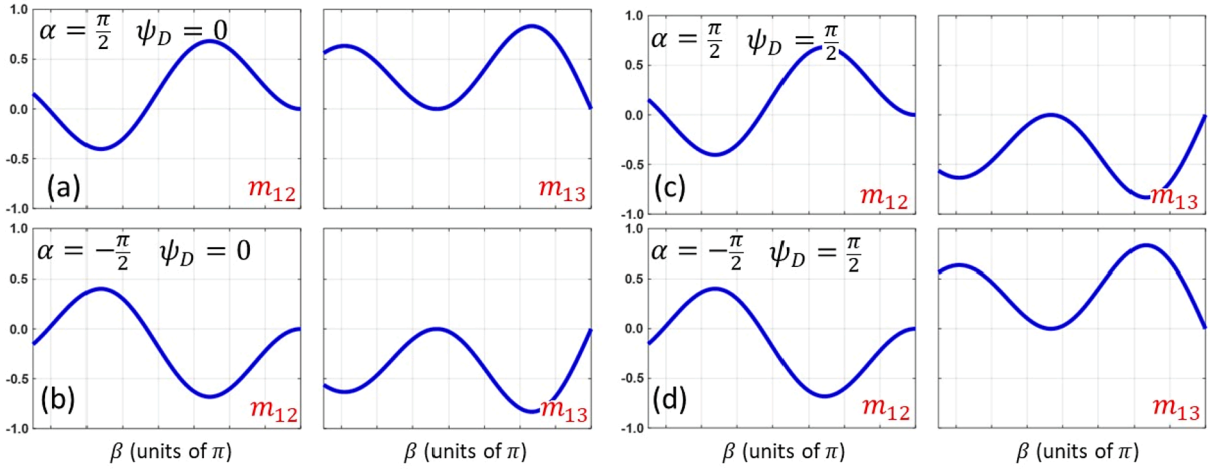

Fig. 4. Evolution of the m_{12} and m_{13} elements of the Mueller matrix with respect to β for a TN-LC cell in the Lu and Saleh model [5] for (a) $\alpha = +\pi/2$, $\psi_D = 0$, (b) $\alpha = -\pi/2$, $\psi_D = 0$, (c) $\alpha = +\pi/2$, $\psi_D = \pi/2$ and (d) $\alpha = -\pi/2$, $\psi_D = \pi/2$.

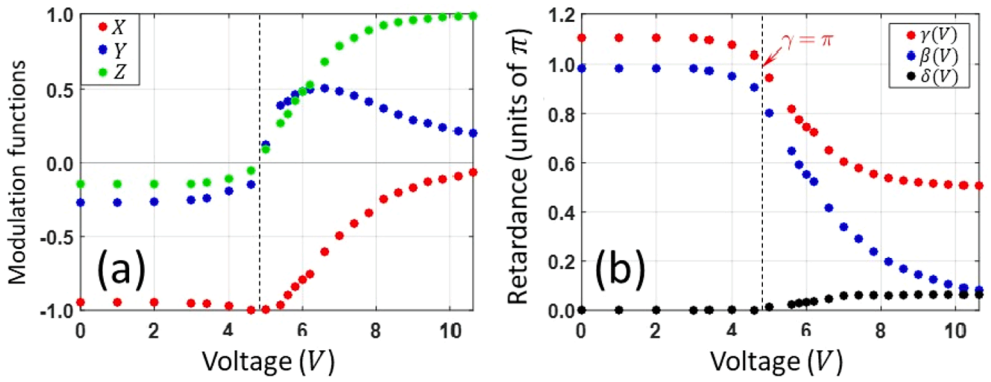

Fig. 5. (a) Experimental values of the modulation functions $X(V)$, $Y(V)$ and $Z(V)$ derived from the diagonal terms of the Mueller matrix in Fig. 3(a). (b) Experimental values of the retardance parameters $\gamma(V)$, $\beta(V)$ and $\delta(V)$ of the microscopic model by Lu & Saleh [5] corrected with the edge layers [7].

the retarder matrix that is obtained by performing the polar decomposition to the experimental Mueller matrix. For low voltages, the Lu and Saleh model is very accurate and $\delta = 0$. The experimental values of X, Y, Z for $V = 0$ allow obtaining the maximum value of the Lu and Saleh parameters through Eq. (4), giving the result $\gamma_{max} = 1.10\pi$, and $\beta_{max} = \sqrt{\gamma_{max}^2 - \alpha^2} = 0.98\pi$ (where we took $\alpha = \pi/2$).

For other voltages we first consider $Z = (\alpha \sin\gamma)/\gamma$ to obtain the evolution with the applied voltage of $\gamma(V)$ and $\beta(V) = \sqrt{(\gamma(V))^2 - \alpha^2}$. Note that the Z function is insensitive to the edge layers. Hence, the curves $X(V)$, $Y(V)$ are employed to determine the edge layer retardance parameter $\delta(V)$ from Eq. (27a), (27b). Fig. 5(b) illustrates the result, which shows the expected behavior. The adiabatic point where $\gamma(V) = \pi$ has been marked.

4. Simplified procedure

The previous polarimetric characterization reveals that the Mueller matrix is very useful to provide the full characterization of the TN-LC cell parameters. The ability to decouple the measurement of the twist angle (α), the cell orientation (ψ_D) and the maximum retardance (β_{max}) is particularly interesting since such independent measurement avoids possible ambiguities. Therefore, calibration with multiple wavelengths is not necessary. The experimental Mueller matrix in Fig. 3 also enables predicting the transmission at any other polarization configuration. However, the experimental determination of the Mueller matrix does require several measurements (in this case 6×6 measurements for each voltage).

Therefore, we propose a simplified approach, based on the assumption that the TN-LC cell is a pure retarder component (devoid of depolarization, diattenuation or polarizance), which proves to be accurate enough. This simplified approach consists in the following steps:

Step 1: First, TN-LC cell must be placed between crossed circular polarizers; in this situation the normalized transmission is given by $T_1 = T_{C\perp} = Y^2$ (Eq. (19)). This equation holds independently of any rotation of the device, thus being valid when the cell is not aligned with the reference framework ($\psi_D \neq 0$). When reaching the local adiabatic point, the cell acts as a pure polarization rotator, and the output polarization remains circularly polarized orthogonal to the circular analyzer. Hence, null transmission is obtained which can be easily observed, even with the naked eye. Then, with the cell tuned at the adiabatic point, it is illuminated with linearly polarized light, and the rotation of the polarization plane provides the twist angle α. Again, this measurement can be done with the naked eye, since a linear polarizer can be used to seek for null transmission before and behind the LC cell. The sign of α can be easily determined by detuning the LC cell from the adiabatic point and detecting the sense of the polarization rotation.

Step 2: Once the twist angle is retrieved, the orientation of the LC director at the input surface (ψ_D) can be found by searching for the orientation of the polarization eigenstates, as previously explained in Fig. 3. However, this requires measuring the Mueller matrix. An alternative approach consists in placing the cell between parallel linear polarizers and change the relative angle [10]. In this situation, if the parallel polarizers are not aligned with the LC director then $\xi_1 = \xi_2 = \psi_D$ and Eq. (18) becomes.

$$T_L(\xi_1 = \xi_2) = (X\cos\alpha + Z\sin\alpha)^2 + (Y\cos(2\psi_D - \alpha))^2 \tag{29}$$

Upon applying a constant voltage and taking measurements by rotating the LC cell the curve $T_L(\psi_D)$ is a sinusoidal function with the maxima located at $\psi_D = \alpha/2$ and $\psi_D = \alpha/2 + \pi/2$. The remaining ambiguity on which of these two values corresponds to the LC director can be resolved by setting a linear analyzer at 0° and illuminating the LC with input linearly polarized light at 45° and with right circularly polarized light. For a pure retarder element, these configurations provide a transmission given by $T = (1 + m_{12})/2$ and $T = (1 + m_{13})/2$ respectively, so the same kind of reasoning as in Fig. 4 can be applied.

Step 3: Finally, placing the cell between linear polarizers but now with angles $\xi_1 = 0$ (parallel to the input LC director orientation) and $\xi_2 = \alpha + \pi/2$ (crossed to the output LC director orientation), Eq. (19) becomes $T_2 = Z^2$. Then, by setting the linear polarizers at $\xi_1 = \pi/4$ and $\xi_2 = \alpha + \pi/4$, Eq. (19) reduces to the relation $T_3 = X^2$.

Fig. 6 shows the results of this simplified procedure. The blue curve in Fig. 6(a) corresponds to the transmission $T_1 = Y^2$ between crossed circular polarizers. It easily identifies the local adiabatic point at the expected value of 4.6 Vpp where a null transmission is obtained. This curve is invariant to the orientation of the LC cell. The twist angle $\alpha = \pi/2$ is measured simply by measuring the rotation induced on linearly polarized light at this voltage. Then, Fig. 6(b) shows the experiment where the LC cell is placed between parallel linear polarizers, so the cell orientation can be found. Here, instead of rotating the TN-LC cell, the two polarizers were simultaneously rotated from zero to 180°. The oscillatory curve expected from Eq. (29) is obtained, with the maxima located at the orientations $\xi = 45°$ and $\xi = 135°$ as expected for a cell with $\alpha = \pi/2$. Once the ambiguities have been resolved, the two remaining curves in Fig. 6(a), corresponding to the transmission $T_2 = Z^2$ and $T_3 = X^2$, can be measured. If required, these data in Fig. 6(a), can be used to retrieve the microscopic retardance parameters $\beta(V)$ and $\delta(V)$, following the procedure described in the previous section.

Finally, we test and confirm the ability of the technique to predict other polarization configurations not employed in the calibration. For this purpose, we calculate the transmission for an arbitrary configuration. Fig. 6(c) and 6(d) compare the prediction and the experimental measurement, for two different configurations. The predictions are drawn as continuous curves, while the green dots indicate the corresponding measurements. In the predictions we use two approaches: one based on the measured Mueller matrix presented in Fig. 3. The second

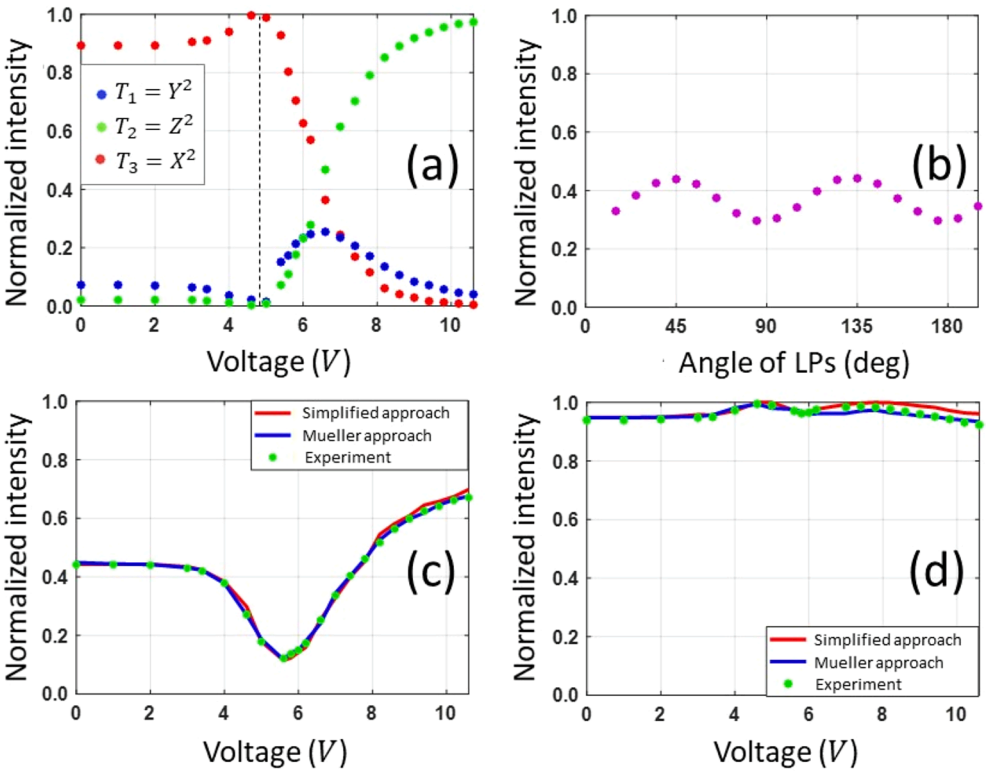

Fig. 6. (a) Normalized transmission of the TN-LC cell placed between crossed circular polarizers $T_2 = Y^2$ and between linear polarizers with transmissions $T_2 = Z^2$ and $T_3 = X^2$. (b) Normalized transmission between parallel linear polarizers as a function of the polarizers' angle. Predictions of the Mueller matrix approach and of the simplified approach and experimental measurement on the transmitted intensity of (c) the configuration with linear polarizers at ($\xi_1 = 30°, \xi_2 = 60°$) and (d) the average rotated eigenvector configuration.

one is based on the calibration of the $X(V)$, $Y(V)$, and $Z(V)$ functions within the simplified approach. First, Fig. 6(c) shows a configuration with linear polarizers oriented at $\xi_1 = 30°$ and $\xi_2 = 60°$. There is an almost perfect coincidence between the experiment and the predictions using the Mueller matrix approach and the simplified approach.

Fig. 6(d) shows the configuration of the average rotated polarization eigenstates. This configuration corresponds to the eigenstates of the **M** matrix in Eq. (3) and it was highly employed for operating TN-LC SLMs as phase-only modulators [27,28]. In this configuration, the TN-LC cell is placed between two QWPs, aligned with the fast axis parallel to the LC director on each side of the cell, and the input and output polarizers form angles $+\zeta$and $-\zeta$ with respect to these directions. In our device we used input and output QWP oriented with angles 0 and $\pi/2$ respectively, and the highest uniform transmission was obtained when setting the polarizers at $\xi_1 = +\zeta = 35°$ and $\xi_2 = \pi/2 - \zeta = 55°$. The agreement is excellent, confirming the accuracy in the characterization process. Note that the prediction of the Mueller matrix is more accurate, as expected. Nevertheless, the simplified procedure also provides very good results.

5. Conclusions

In summary, we have provided a complete polarimetric review of the TN-LC cell. We considered the Jones matrix microscopic models and extended them to the Mueller-Stokes formalism. Based in this review we outline a procedure to fully characterize the modulator and its physical parameters based on the Mueller matrix polarimetric measurement. The calculation of the retardance vector and the polarization eigenstates reveals the orientation of the LC director ψ_D. The identification of the local adiabatic point, where the device operates as a pure polarization rotator, allows finding the twist angle α. Therefore, a characterization of the physical parameters α, ψ_D is achieved with a single wavelength and without requiring a simultaneous fit of a set of different curves unlike other approaches [9,10]. Furthermore, the proposed Mueller matrix technique easily resolves the ambiguity in the sign of α and in the identification of the fast axis.

Once the TN-LC is aligned with the LC director parallel to the reference framework, the diagonal elements of the Mueller matrix provide the evolution of the $X(V)$, $Y(V)$ and $Z(V)$ functions. These functions can be directly related to the microscopic retardance parameters, the $\beta(V)$ retardance function in the Lu and Saleh standard model [5] and the correction $\delta(V)$ edge layer retardance parameter [7]. Again, these two parameters are measured decoupled, since $\beta(V)$ is determined from the $Z(V)$ function, while $\delta(V)$ is determined from the $X(V), Y(V)$ functions. The whole process can be applied with a single wavelength.

Although complete Mueller matrix polarimetry requires many measurements (here we did 6×6 measurements), valuable information can be obtained from simplified experiments. In addition, the use of polarimetric cameras helps reducing the number of measurements, as in the imaging Mueller matrix polarimeter we recently developed [38] where 12 measurements suffice. Finally, a simplified version of the technique is proposed assuming that the cell is a pure retarder component. This simplified technique can help to rapidly calibrate and configure TN-LC modulators for a desired optical modulation response.

CRediT authorship contribution statement

Esther Nabadda: Investigation, Visualization, Writing – original draft. **Guadalupe López-Morales:** Investigation, Visualization, Methodology, Validation. **David Marco:** Methodology, Validation. **María del Mar Sánchez-López:** Methodology, Validation, Supervision, Writing – review & editing. **Ignacio Moreno:** Conceptualization, Validation, Supervision, Writing – review & editing.

Declaration of Competing Interest

The authors declare that they have no known competing financial interests or personal relationships that could have appeared to influence the work reported in this paper.

Data availability

No data was used for the research described in the article.

Acknowledgements

We acknowledge funding from Ministerio de Ciencia, Innovación y Universidades from Spain (RTI2018-097107-B-C33). Esther Nabadda acknowledges a grant from Generalitat Valenciana, Santiago Grisolia Program (ref. GRISOLIAP/2020/004).

References

[1] N. Konforti, E. Marom, S.-T. Wu, Phase-only modulation with twisted nematic liquid-crystal spatial light modulators, Opt. Lett. 13 (3) (1988) 251–253.
[2] R.K. Komanduri, K.F. Lawler, M.J. Escuti, Multi-twist retarders: broadband retardation control using self-aligning reactive liquid crystal layers, Opt. Express 21 (1) (2013) 404–420.
[3] A. Yariv, P. Yeh, "Light propagation in twisted anisotropic media", Section 5.4 in Optical Waves in Crystals, John Wiley & Sons, New York, 1984.
[4] R.C. Jones, A new calculus for the treatment of optical systems: VII. Properties of the N-matrices, J. Opt. Soc. Am. 38 (8) (1948) 671–685.
[5] K. Lu, B.E.A. Saleh, Theory and design of the liquid crystal TV as an optical spatial phase modulator, Opt. Eng. 29 (3) (1990) 240–246.
[6] J.A. Coy, M. Zaldarriaga, D.F. Grosz, O.E. Martinez, Characterization of a liquid crystal television as a programmable spatial light modulator, Opt. Eng. 35 (1) (1996) 15–19.
[7] A. Marquez, J. Campos, M.J. Yzuel, I. Moreno, J.A. Davis, C. Iemmi, A. Moreno, A. Robert, Characterization of edge effects in twisted nematic liquid crystal displays, Opt. Eng. 39 (12) (2000) 3301–3307.
[8] M. Yamauchi, Jones-matrix models for twisted-nematic liquid-crystal devices, Appl. Opt. 44 (21) (2005) 4484–4493.
[9] R. Giust, J.-P. Goedgebuer, Determination of the twist angle and the retardation properties of twisted nematic liquid crystal television by spectral measurements, Opt. Eng. 37 (2) (1998) 629–634.
[10] J.A. Davis, D.B. Allison, K.G. D'Nelly, M.L. Wilson, I. Moreno, Ambiguities in measuring the physical parameters for twisted-nematic liquid-crystal spatial light modulators, Opt. Eng. 38 (4) (1999) 705–709.
[11] H. Kim, Y.H. Lee, Unique measurement of the parameters of a twisted-nematic liquid-crystal display, Appl. Opt. 44 (9) (2005) 1642–1649.
[12] V. Durán, J. Lancis, E. Tajahuerce, Z. Jaroszewicz, Cell parameter determination of a twisted-nematic liquid crystal display by single-wavelength polarimetry, J. Appl. Phys. 97 (4) (2005) 043101.
[13] I. Moreno, A.M. Cutillas, M.M. Sánchez-López, P. Velásquez, F. Mateos, Full prediction of the broadband optical modulation performance of a twisted nematic liquid crystal cell, Opt. Commun. 281 (22) (2008) 5520–5526.
[14] J.A. Davis, P. Tsai, K.G. D'Nelly, I. Moreno, Simple technique for determining the extraordinary axis direction for twisted nematic liquid crystal spatial light modulator, Opt. Eng. 38 (5) (1999) 929–932.
[15] I. Moreno, P. Velásquez, C.R. Fernández-Pousa, M.M. Sánchez-López, F. Mateos, Jones matrix method for predicting and optimizing the optical modulation properties of a liquid-crystal display, J. Appl. Phys. 94 (6) (2003) 3697–3702.
[16] A.J. Macfaden, T.D. Wilkinson, Characterization, design, and optimization of a two-pass twisted nematic liquid crystal spatial light modulator system for arbitrary complex modulation, J. Opt. Soc. Am. A 34 (2) (2017) 161–170.
[17] V. Durán, J. Lancis, E. Tajahuerce, Equivalent retarder-rotator approach to on-state twisted nematic liquid crystal displays, J. Appl. Phys. 99 (2006), 113101.
[18] D. Goldstein, Polarized Light, 3rd edition, CRC Press, 2010.
[19] J.E. Wolfe, R.A. Chipman, Polarimetric characterization of liquid-crystal-on-silicon panels, Appl. Opt. 45 (8) (2006) 1688–1703.
[20] A. Márquez, I. Moreno, C. Iemmi, A. Lizana, J. Campos, M.J. Yzuel, Mueller-Stokes characterization and optimization of a liquid crystal on silicon display showing depolarization, Opt. Express 16 (3) (2008) 1669–1685.
[21] R.S. Verma, M.K. Swami, S.S. Manhas, P.K. Gupta, Mueller matrix-based optimization of reflective type twisted nematic liquid crystal SLM at oblique incidences, Opt. Commun. 283 (12) (2010) 2580–2587.
[22] K. Dev, A. Asundi, Mueller–Stokes polarimetric characterization of transmissive liquid crystal spatial light modulator, Opt. Lasers Eng. 50 (4) (2012) 599–607.
[23] Z. Zhang, Z. You, D. Chu, Fundamentals of phase-only liquid crystal on silicon (LCOS) devices, Light: Sci. Appl. 3 (10) (2014) e213.
[24] F.J. Martínez, A. Márquez, S. Gallego, J. Francés, I. Pascual, A. Beléndez, Retardance and flicker modeling and characterization of electro-optic linear retarders by averaged Stokes polarimetry, Opt. Lett. 39 (4) (2014) 1011–1014.
[25] I. Moreno, A. Lizana, J. Campos, A. Marquez, C. Iemmi, M.J. Yzuel, Combined Mueller and Jones matrix method for evaluation of the complex modulation in liquid-crystal-on-silicon display, Opt. Lett. 33 (6) (2008) 627–629.
[26] J.L. Pezzaniti, R.A. Chipman, Phase-only modulation of a twisted nematic liquid-crystal TV by use of the eigenpolarization states, Opt. Lett. 18 (18) (1993) 1567–1569.
[27] J.A. Davis, I. Moreno, P. Tsai, Polarization eigenstates for twisted-nematic liquid crystal displays, Appl. Opt. 37 (5) (1998) 937–945.
[28] I. Moreno, J.A. Davis, K.G. D'Nelly, D.B. Allison, Transmission and phase measurements for polarization eigenvectors in twisted-nematic liquid-crystal spatial light modulators, Opt. Eng. 37 (11) (1998) 3048–3052.
[29] J. Nicolás, J. Campos, M.J. Yzuel, Phase and amplitude modulation of elliptic polarization states by non-absorbing anisotropic elements: application to liquid-crystal devices, J. Opt. Soc. Am. A 19 (5) (2002) 1013–1020.
[30] B.E.A. Saleh, M.C. Teich, Fundamentals of Photonics, 2nd Edition,, John Wiley and Sons Inc., 2007.
[31] C.R. Fernández-Pousa, I. Moreno, N. Bennis, C. Gómez-Reino, Generalized formulation and symmetry properties of anisotropic devices. Application to liquid crystal displays, J. Opt. Soc. Am A 17 (11) (2000) 2074–2080.
[32] Z. Zhuang, Y.J. Kim, J.S. Patel, Achromatic linear polarization rotator using twisted nematic liquid crystals, Appl. Phys. Lett. 76 (26) (2000) 3995–3997.
[33] I. Moreno, N. Bennis, J.A. Davis, C. Ferreira, Twist angle determination in liquid crystal displays by location of local adiabatic points, Opt. Commun. 158 (1–6) (1998) 231–238.
[34] R.A. Chipman, Mueller matrices, Ch. 14 in *Handbook of Optics*, Vol. 1, third ed., in: M. Bass, V.N. Mahajan (Eds.) McGraw-Hill, New York (2010).
[35] S.Y. Lu, R.A. Chipman, Interpretation of Mueller matrices based on polar decomposition, J. Opt. Soc. Am. A 13 (5) (1996) 1106–1113.
[36] S. Manhas, M.K. Swanmi, P. Buddhiwant, N. Ghosh, P.K. Gupka, K. Singh, Mueller matrix approach for determination of optical rotation in chiral turbid media in backscattering geometry, Opt. Express 14 (1) (2006) 190–202.
[37] O. Arteaga, A. Canillas, Pseudopolar decomposition of the Jones and Mueller-Jones exponential polarization matrices, J. Opt. Soc. Am A 26 (4) (2009) 783–793.
[38] G. López-Morales, M.M. Sánchez-López, A. Lizana, I. Moreno, J. Campos, Mueller matrix polarimetric imaging analysis of optical components for the generation of cylindrical vector beams, Crystals 10 (12) (2020) 1155.